Density Oscillator: Analysis of Flow Dynamics and Stability

O. Steinbock,[1] A. Lange,[2] and I. Rehberg[1]

[1]*Universität Magdeburg, Institut für Experimentelle Physik, Universitätsplatz 2, D-39106 Magdeburg, Germany*
[2]*Universität Magdeburg, Institut für Theoretische Physik, Universitätsplatz 2, D-39106 Magdeburg, Germany*
(Received 2 March 1998)

Two open containers filled with fluids of different density and connected by a vertical capillary tube can approach their thermodynamical equilibrium via an oscillatory flow. The temporal evolution of flow velocities was measured quantitatively. Data on the critical values determining the flow reversal are extracted yielding a simple dependence of the critical level of heavy fluid as a function of the density ratio and the length of the capillary. A novel theoretical description of the system is presented which is based on a one-fluid model and a steady-state approximation for a two-dimensional flow. Theoretical results are in good agreement with the experimental data.   [S0031-9007(98)06728-3]

The investigation of fluid dynamics and hydrodynamic instabilities has experienced a renaissance in modern physics [1]. The research often fruitfully combines classical concepts with novel approaches from nonlinear dynamics and enhances our understanding of phenomena that are typically studied in fields such as oceanography, meteorology, or geophysics [2]. While this applied research focuses mainly on the dynamics in infinite systems, certain hydrodynamic instabilities are strongly related to the presence of spatial constraints. A fascinating example is the density oscillator that was discovered by Martin [3]. It combines the unstable stratification of two fluids known from Rayleigh-Taylor experiments [4] with the spatiotemporal constraints of the ordinary Poiseuille flow. Because of its experimental simplicity and high degree of reproducibility, it also appears to be an excellent model system for the study of self-induced relaxation oscillations [2,5].

The density oscillator consists of two containers separating the fluids (Fig. 1). The inner and outer containers hold the dense and light fluids, respectively. The small inner container has a vertical capillary tube attached to its bottom that allows the dense fluid to flow into the large container and vice versa. Typical fluids are aqueous NaCl solutions (density ρ_s) and water (ρ_w) [3,6,7]. Surprisingly, one finds an oscillatory flow through the capillary giving rise to beautiful jets of ascending water and descending salt water. The jets and their oscillatory change of flow direction can be easily followed with the naked eye due to differences in refraction.

An important finding of Martin [3] was the distinction between two limiting cases: While fast oscillations are subject to the influence of inertia, slow oscillations as studied in this Letter can be described in terms of steady-state approximations. In both cases, two unstable situations can be distinguished for which the static pressures are balanced: During the phase of heavy fluid flowing downwards, the capillary is filled entirely with this fluid and its level $h(t)$ in the small container is decreasing. The system is approaching an unstable pressure equilibrium at

$h(t) = h_1$ that is given by

$$\rho_w gH = \rho_s gh_1. \tag{1}$$

For the opposite case, the tube contains only light fluid and is targeting a different pressure equilibrium which is realized for a salt water level h_2:

$$\rho_w g(H - L) = \rho_s g(h_2 - L). \tag{2}$$

If we consider H to be constant the unstable equilibrium levels h_1 and h_2 define the tidal amplitude levels as

$$\Delta h = h_2 - h_1 = L(1 - \rho_w/\rho_s). \tag{3}$$

Other investigations of the density oscillator include modifications where the capillary tube is replaced by a hole or the originally miscible fluids are replaced
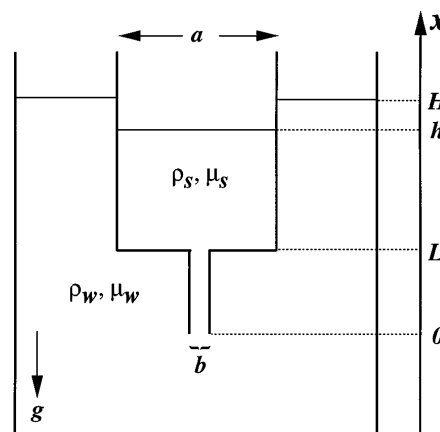

FIG. 1.   Schematic drawing of the experimental setup. The outer container ($V = 25$ l, filled with water) is much larger than the inner container that hosts the salt water. Therefore, the height of the water level H can be assumed to be constant. The inner container is cylindrical with an inner diameter of $a = 34.2$ mm. A capillary tube oriented vertically (i.e., parallel to the gravity acceleration g) connects both reservoirs. The parameters b ($b = 0.74$ mm) and L denote the inner diameter and the length of the capillary, respectively. ρ and μ denote densities and dynamic viscosities, respectively. The indices w and s correspond to water and salt water.

by immiscible liquids [7–9]. The latter modification introduces additional forces due to surface tension that were avoided in our investigations.

This Letter presents quantitative measurements of the height evolution $h(t)$. Critical heights and flow velocities characterizing the state of flow reversal are presented. The experimental results are compared with calculations that address the key problem of how to derive the conditions for flow reversal from the unstable pressure equilibria. The calculations follow an approach that has been successfully used for a particular example of heat transfer [10].

Dimensions and parameters specifying the experimental setup are indicated in Fig. 1. The results presented in the following have been obtained by varying the length L of the capillary tube in a range of 1 to 10 cm. The density ratio of salt water ([NaCl] = 1–5 M) to pure water was varied from 1.03 to 1.18. All experiments were carried out at room temperature. The salt water level was monitored by a CCD camera.

Figure 2 shows a typical example for the temporal evolution of the height $h(t)$. According to the direction of the oscillatory flow, one observes increasing or decreasing values of h. The period of oscillations (1590 ± 10 s in Fig. 2) is constant for many cycles, since salt water accumulates primarily at the bottom of the large container, while the light fluid accumulates at the top of the inner container. The dashed lines represent simple exponential fits to the successive branches of upflow and downflow. The good agreement between experimental data and calculated fits stems from the characteristics of the Poiseuille flow within the capillary. The Hagen-Poiseuille equation relating the volume flux to the driving pressure difference yields a first-order differential equation in h and allows

the extraction of the corresponding relaxation time τ:

$$\frac{1}{\tau} = \frac{(b/2)^4 \rho g}{8a^2 \mu L}, \qquad (4)$$

where $\rho = \rho_s$ and $\mu = \mu_s$ for the example of salt water flowing downwards.

The experimental data also reveal a slow, but continuous shift of h toward higher values. This shift is strongly related to the pressure equilibria discussed above: While the unstable pressure equilibria remain essentially constant, the volume reduction during the downflow of salt water has to be compensated by a larger volume of water. The validity of Eq. (3) was verified in additional experiments, where L and ρ_s were varied systematically. Experimental data on Δh were obtained from the asymptotic values of the exponential fits for successive upflow and downflow phases. For the example shown in Fig. 2 this value is found to be $\Delta h_{\text{expt}} = 5.3 \pm 0.2$ mm, which is in good agreement with the expected value of 5.2 mm.

Figure 3 shows some data on the dependence of the relaxation time τ on the length L of the capillary tube for constant densities. Solid circles and diamonds represent experimental data obtained for the relaxation time of salt water and pure water, respectively. Linear fits of these data are indicated by dashed lines. The density ratio and viscosity of salt water ([NaCl] = 4 M) were measured to be $\rho_s/\rho_w = 1.153$ and $\mu_s = 1.5$ mPa s. Based on these data, the straight lines in Fig. 3 represent the expected relaxation times according to Eq. (4). Experimental and theoretical data are in good agreement. However, a small negative offset is found in our experiments that could indicate small deviations from an ideal Poiseuille flow or pinning of the salt water meniscus.
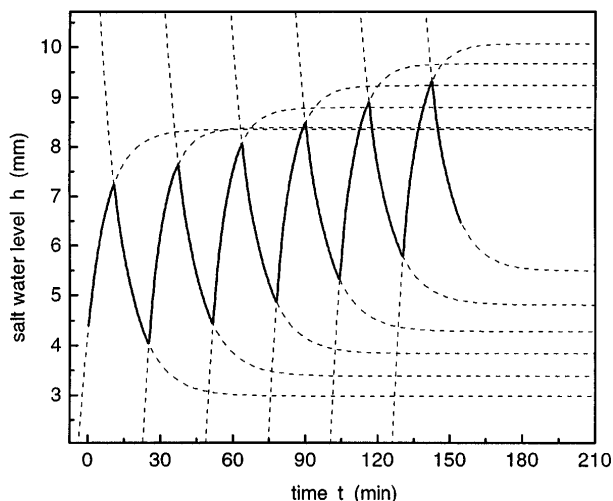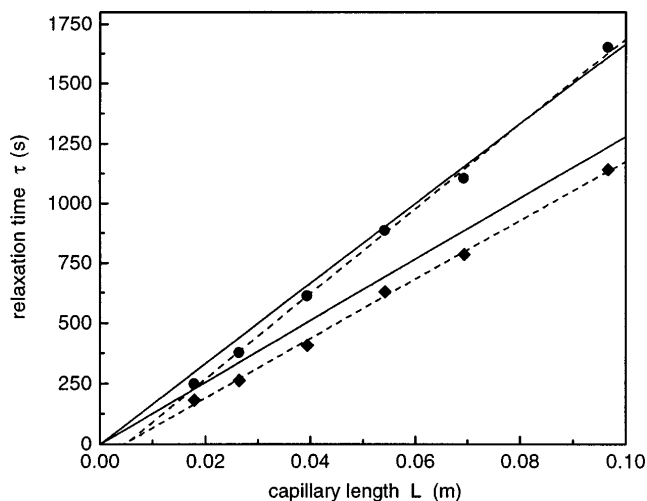

FIG. 2. A typical example of temporal evolution of the level of salt water $h(t)$ as observed in the inner container (solid curve). The dashed curves represent exponential fits for the successive phases of the oscillatory flow: $h(t) \propto [\exp(-t/\tau) + \text{const}]$. The length of the capillary tube: $L = 3.94$ cm.

FIG. 3. Relaxation times τ as a function of the capillary length obtained from experiments similar to the one shown in Fig. 2. Solid circles and diamonds represent experimental data for the change from upflow to downflow and vice versa, respectively. Dashed lines indicate the result of the linear regression of experimental data. Straight lines represent the expected dependences based on Eq. (4).

In order to obtain a better understanding of the spatiotemporal dynamics during the flow reversal, additional experiments have been performed in which the heavy fluid was stained with red ink. This procedure allows one to easily monitor the salt water jet at the periphery of the bottom orifice of the capillary [3]. A few seconds prior to the flow reversal one observes that a small water bubble is penetrating the capillary at a small section close to its boundary. The bubble grows rapidly to a water column occupying approximately one-half of the cross section of the capillary tube. At this stage the salt water jet is still present, but reduced in size. When the unstained water has climbed up to the upper end of the capillary it terminates the salt water inflow immediately. Notice that this flow reversal lasts only a few seconds, while under our experimental conditions the oscillation period is in the range of 10 to 40 min.

An obvious idea to apply to the problem of flow reversal is the Rayleigh-Taylor instability of two differently dense *viscous* fluids. A rigorous treatment would require calculations in three-dimensional cylindrical coordinates. The resulting equations with the appropriate boundary conditions present a severe problem to solve analytically. Therefore a theoretical description is derived on the basis of a one-fluid model in a two-dimensional rectangular geometry. Since the critical level h_c is determined by the *local* velocity field at the tube orifice (see experimental observation and below), this approximation seems reasonable. The analysis focuses on the downflow of salt water since the analogous treatment of the upflow of water is obvious. The stationary laminar flow is considered in a duct of length L and width b. The flow can be considered as two dimensional if one assumes that the depth of the duct is large compared to its width. The downflow is disturbed at the lower end of the left duct wall by water which tries to rise against the downflowing salt water. To describe such a disturbance in the frame of a one-fluid model, a dimensionless function $\Theta(x, y), 0 \le \Theta(x, y) \le 1$ is introduced where x and y denote the vertical and horizontal coordinate, respectively. Θ mediates the continuous transition between water and salt water, i.e., $\rho = \rho_s + (\rho_w - \rho_s)\Theta$ and $c = 1 - \Theta$, where c is the concentration of salt water in the fluid.

The equations governing this system are the equation of continuity, $\text{div } \vec{v} = 0 = \partial_x u + \partial_y v$, the x and y component of the Navier-Stokes equation, and the diffusion equation

$$u\partial_x u + v\partial_y u = -g + g\frac{(\rho_s - \rho_w)\Theta}{\rho_s} - \frac{1}{\rho_s}\partial_x p + \nu_s(\partial_x^2 u + \partial_y^2 u), \qquad (5)$$

$$u\partial_x v + v\partial_y v = -\frac{1}{\rho_s}\partial_y p + \nu_s(\partial_x^2 v + \partial_y^2 v), \quad (6)$$

$$u\partial_x c + v\partial_y c = D(\partial_x^2 c + \partial_y^2 c). \qquad (7)$$

The diffusion equation is needed to deal with the two fluids in a one-fluid model. The vertical (horizontal) velocity component in the x (y) direction is u (v), p is the pressure, g is the gravity acceleration, ν_s is the kinematic viscosity of salt water, and D is its diffusion coefficient. The second term on the right-hand side in Eq. (5) describes the disturbance of the downflow. The Boussinesq approximation was used in the equations of motion by treating $\rho = \rho_s$ as a constant in all terms except for the one in the disturbing force. For $\Theta = v = \partial_x u = 0$ the Poiseuille flow profile in a duct with $Q = -[b^3/(12\mu_s)]\partial_x P$ is recovered. The pressure difference $\partial_x P$ in the flow rate Q is determined by gravity only since both vessels are open to atmospheric pressure.

The governing equations can be written in a nondimensional form by introducing $\overline{x} = x/L$, $\overline{y} = y/b$, $\overline{u} = ub/Q$, $\overline{v} = vL/Q$, and $\overline{p} = pb^3/\rho_s L\nu_s Q$. In the new variables, the equation of continuity becomes $\partial_{\overline{x}}\overline{u} + \partial_{\overline{y}}\overline{v} = 0$ and Eqs. (5)–(7) read

$$\text{Re}\,\varepsilon(\overline{u}\partial_{\overline{x}}\overline{u} + \overline{v}\partial_{\overline{y}}\overline{u}) = \alpha\Theta - \beta - \partial_{\overline{x}}\overline{p}$$
$$+ \varepsilon^2\partial_{\overline{x}}^2\overline{u} + \partial_{\overline{y}}^2\overline{u}, \qquad (8)$$

$$\text{Re}\,\varepsilon^3(\overline{u}\partial_{\overline{x}}\overline{v} + \overline{v}\partial_{\overline{y}}\overline{v}) = -\partial_{\overline{y}}\overline{p} + \varepsilon^4\partial_{\overline{x}}^2\overline{v} + \varepsilon^2\partial_{\overline{y}}^2\overline{v}, \qquad (9)$$

$$\varepsilon(\overline{u}\partial_{\overline{x}}\Theta + \overline{v}\partial_{\overline{y}}\Theta) = \frac{D}{Q}\varepsilon^2\partial_{\overline{x}}^2\Theta + \partial_{\overline{y}}^2\Theta. \qquad (10)$$

The Reynolds number $\text{Re} = Q/\nu_s$, $\varepsilon = b/L$, $\beta = gb^3/(\nu_s Q)$, and the control parameter

$$\alpha = \frac{gb^3}{\nu_s Q}\left(1 - \frac{\rho_w}{\rho_s}\right) \qquad (11)$$

were introduced. The control parameter α contains the two counteracting quantities flow rate Q and density difference $(1 - \rho_w/\rho_s)$. Since the flow is two dimensional, we define a stream function $\Psi(\overline{x}, \overline{y})$, $\overline{u} = \partial_{\overline{y}}\Psi(\overline{x}, \overline{y})$ and $\overline{v} = -\partial_{\overline{x}}\Psi(\overline{x}, \overline{y})$, by which the equation of continuity is automatically fulfilled. The boundary conditions in terms of Ψ are $\partial_{\overline{y}}\Psi = -\partial_{\overline{y}\overline{x}}\Psi = 0$ (no slip) and $-\partial_{\overline{x}}\Psi = 0$ (no penetration of the vertical walls) at $\overline{y} = 0, 1$. The constant flow rate is ensured by $\Psi = 1$ at $\overline{y} = 1$ and $\Psi = 0$ at $\overline{y} = 0$. According to the observed evolution of the water bubble, $\Theta(\overline{x}, \overline{y})$ has to be equal to 1 at $\overline{x} = \overline{y} = 0$ and equal to zero at $\overline{y} = 1$.

Since the length L of the duct is very large compared to its width b, the remaining unknown functions Ψ, Θ, and $\overline{p}$ are expanded in terms of the small parameter ϵ [10]. In lowest order, the solution $\Theta_0(\overline{x}, \overline{y}) = \vartheta_0(\overline{x})(1 - \overline{y})$ and $\Psi_0(\overline{x}, \overline{y}) = 3\overline{y}^2 - 2\overline{y}^3 + (\alpha/24)\vartheta_0(\overline{x})(1 - \overline{y})^2\overline{y}^2$ satisfies all boundary conditions. The unspecified function $\vartheta_0(\overline{x})$ with $\vartheta_0(0) = 1$ is free for modeling the decreasing concentration of water in the down-flowing fluid in the $\overline{x}$ direction. The instability occurs if the derivative of the velocity in the $\overline{x}$ direction changes its sign at the lower
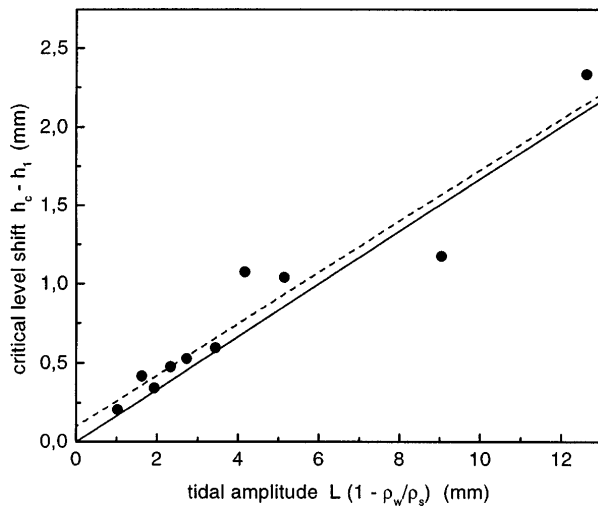
FIG. 4. Characterization of the change from downflow to upflow. The height difference $h_c - h_1$ corresponds to the height of the salt water level above the unstable equilibrium h_1 at which the flow direction changes. Solid circles: experimental data obtained for different values of L and ρ_s. Dashed line: linear regression of experimental data. Straight line: expected dependence as given in Eq. (12).

end of the left tube wall. This local counterflow expands rapidly because the flow rate decreases due to the falling level of salt water in the small container. Thus, $\partial_{\bar{y}}^2 \Psi = 0$ at $\bar{x} = \bar{y} = 0$ gives the critical parameter $\alpha_c = -72$ and defines therefore the threshold for the stability of the downflow. Inserting the Poiseuille flow profile, the critical pressure difference $\partial_x P = g(h_c \rho_s - H \rho_w)/L$, and α_c in (11) leads to

$$ h_c - h_1 = \frac{1}{6}\left(1 - \frac{\rho_w}{\rho_s}\right)L \, . \tag{12} $$

Equation (12) expresses the difference between the unstable equilibrium level h_1 (1) and the critical level h_c, where the downflow actually reverses. Concerning the geometry, this difference depends only on the length L but is independent of the cross section of the tube. Therefore, there is an excellent agreement between the theoretical and experimental values in the height difference versus tidal amplitude plot (Fig. 4). Comparing the slopes, the theoretical value of $1/6$ is very near to the fit value of

0.16 ± 0.02 from the experimental data. The shift of the observed data towards higher values of $h_c - h_1$ could be caused by uncontrolled perturbations of the system (e.g., small mechanical vibrations) which induce premature flow reversals.

A similar two-dimensional calculation in cylindrical coordinates would correspond to an axial-symmetrical disturbance at the orifice of the tube. Because such a type of disturbance has never been observed in the experiments, one has to extend to three-dimensional calculations. Therefore our proposed analytical analysis is limited to a two-dimensional rectangular geometry.

For the presented hydrodynamic oscillator the distance between unstable pressure equilibria, the exponential flow dynamics, and the critical heights have been measured quantitatively. Furthermore, a thorough theoretical understanding has been achieved. On this basis other oscillator characteristics such as frequencies can be easily determined. Because of its simple experimental setup and theoretical accessibility, we consider this system as an impressive example of oscillatory behavior in hydrodynamics.

[1] T.E. Faber, *Fluid Dynamics for Physicists* (Cambridge University Press, Cambridge, England, 1995).
[2] Steven H. Strogatz, *Nonlinear Dynamics and Chaos* (Addison-Wesley, Reading, MA, 1994).
[3] S. Martin, Geophys. Fluid Dyn. **1**, 143 (1970).
[4] B.A. Remington *et al.,* Phys. Plasma **2**, 241 (1994).
[5] P.S. Landa, *Nonlinear Oscillations and Waves in Dynamical Systems* (Kluwer Academic Publishers, Dordrecht, 1996).
[6] P.-H. Alfredsson and T. Lagerstedt, Phys. Fluids **24**, 10 (1981).
[7] K. Yoshikawa and K. Fukunaga, Chem. Phys. Lett. **174**, 203 (1990).
[8] K. Yoshikawa, N. Oyama, M. Shoji, and S. Nakata, Am. J. Phys. **59**, 137 (1991).
[9] K. Yoshikawa, S. Maeda, and H. Kawakami, Ferroelectrics **86**, 281 (1990).
[10] T. Mahmood and J.H. Merkin, Mass Heat Transfer **24**, 257 (1989).